Do Attractive Polymer–Nanoparticle Interactions Retard Polymer Diffusion in Nanocomposites?

ARTICLE *in* MACROMOLECULES · MAY 2013

Impact Factor: 5.8 · DOI: 10.1021/ma4000557

6 AUTHORS, INCLUDING:

Chia-Chun Lin
University of Pennsylvania
6 PUBLICATIONS **33** CITATIONS
SEE PROFILE

Jeffrey S. Meth
Dupont
61 PUBLICATIONS **1,236** CITATIONS
SEE PROFILE

Karen I Winey
University of Pennsylvania
331 PUBLICATIONS **11,306** CITATIONS
SEE PROFILE

Macromolecules

Article

pubs.acs.org/Macromolecules

Do Attractive Polymer–Nanoparticle Interactions Retard Polymer Diffusion in Nanocomposites?

Chia-Chun Lin,[†] Sangah Gam,[†] Jeffrey S. Meth,[‡] Nigel Clarke,[§] Karen I. Winey,[†] and Russell J. Composto*[,†]

[†]Department of Materials Science and Engineering, University of Pennsylvania, Philadelphia, Pennsylvania 19104-6272, United States

[‡]Central Research & Development, DuPont Co., Wilmington, Delaware, 19880-0400, United States

[§]Department of Physics and Astronomy, University of Sheffield, Sheffield S3 7RH, United Kingdom

Supporting Information

ABSTRACT: Diffusion of deuterated poly(methyl methacrylate) (dPMMA) is slowed down in a PMMA matrix filled with hydroxyl-capped spherical silica nanoparticles, from 13 to 50 nm in diameter and at loadings up to 40 vol %. At constant $T - T_g = 75$ K, the normalized diffusion coefficients (D/D_0) collapse onto a master curve, when plotted against the confinement parameter, $ID/2R_g$, where ID is interparticle distance and $2R_g$ is probe size. This result suggests that the confinement parameter captures the effect of nanoparticle size, size polydispersity, and volume fraction on polymer dynamics for the PMMA composite. For $ID < 2R_g$, the master curve exhibits a strongly confined region where D/D_0 decreases by up to 80%, whereas for $ID > 2R_g$, the curve falls in a weakly confined region where D/D_0 decreases only moderately by up to 15%. Surprisingly, D/D_0 is reduced even when ID is 8 times larger than $2R_g$. A comparison between the master curves for PMMA and polystyrene nanocomposites indicates that attractive interactions in the PMMA system do not significantly alter the center-of-mass diffusion of macromolecules in polymer nanocomposites.

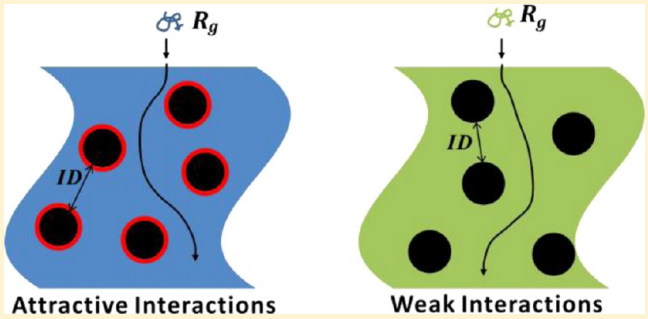

INTRODUCTION

Polymer nanocomposites (PNC) have drawn enormous interest because the addition of nanoparticles to polymers imparts unique properties. Specifically, inorganic nanofillers such as clays have been shown to enhance thermal stability[1] and mechanical strength,[2] whereas noble metal nanoparticles and carbon nanotubes can impart polymers with tunable optical properties[3] and electrical conductivity.[4] Another advantage is that a very small loading of nanofiller can significantly affect properties because of the high interfacial area between matrix and nanofillers.[5,6] For example, 1 vol % of 10 nm nanoparticles has 0.006 nm^2 of surface area per nm^2 of volume; thus, interactions are expected to be very influential. The viscosity of polymers is also influenced by the addition of nanofillers, and correspondingly, the processability of PNCs differ from the pure polymer case.[7,8] Thus, understanding the dynamics of macromolecules in the presence of nanoparticles can provide important insight into understanding processing conditions and flow behavior[9] of the PNC.

Experimental studies of polymer relaxation in PNCs provide conflicting results regarding the effect of nanofillers on polymer dynamics. Moreover, a comprehensive model that incorporates local segmental and long-range center-of-mass relaxations (aka reptation model) is lacking. For example, Bogoslovov et al.[10] investigated the effect of attractive interactions on local dynamics in PNCs containing poly(vinyl acetate) and silica nanoparticles (NPs) and found that the local segmental relaxations near the surface of the nanoparticles are unaffected. On the other hand, studies[11−15] of the glass transition of PNCs having attractive interactions indicate that the mobility of the chains in the vicinity of the nanoparticles are slower than the bulk, thus altering the relaxation behavior. Bound layers immobilized around the NPs having attractive interaction with the matrix polymer have also been investigated.[16−19] For example, Harton et al.[17] showed 1 nm thick bound layers near silica nanoparticles (15 nm) surrounded by poly(2-vinlypyridine) (P2VP) matrix, and the cooperative motion of those unbound P2VP is not strongly affected compared with bulk P2VP.

To describe the role of nanoparticles on the slowest relaxations times, a modified tube model[20] can be invoked where the topological constraints from neighboring chains in an entangled polymer melt are altered by the inclusion of nanoparticles. Simulation and experimental results show that the entanglement density decreases when nanoparticles are added.[21,22] However, studies of the effect of nanofillers on the

Received: January 8, 2013
Revised: April 11, 2013
Published: May 24, 2013

   dx.doi.org/10.1021/ma4000557 | Macromolecules 2013, 46, 4502−4509

viscosity of polymers show different behaviors which crucially depend on nanofiller size relative to polymer radius of gyration (R_g). When the nanoparticles are smaller than R_g, the PNC viscosity decreases, relative to pure polymer, as filler is added.[7,8,23,24] For example, Nusser et al.[23] showed that the viscosity of polydimethylsiloxane (PDMS)/polyhedral oligomeric silisesquioxane (POSS) composites decreases by 15% as POSS content increases to 0.004 and explained this lowering of viscosity due to a constraint release mechanism resulting from the mobility of the nanoparticles. Namely, because of the small size of POSS (~2 nm), the relaxation of the NPs is faster than that of the topological constraint imposed by the polymer melt. When the nanoparticles are larger than R_g, Anderson et al.[25] showed that the viscosity of poly(ethylene oxide) (PEO)/silica (44 nm) increases for PEO matrix polymers having R_g's between 0.8 and 5.9 nm.

Polymer diffusion is slowed down by spherical nanoparticles that have nearly neutral or weak interactions with nearby polymer segments. In our previous study,[26] elastic recoil detection (ERD) was used to investigate the tracer diffusion of deuterated polystyrene (dPS) into polystyrene (PS) mixed with phenyl-capped silica nanoparticles having a diameter of 29 nm. Because of the weak NP−PS interaction and immobile NPs, dispersions up to 50 vol % were achieved, allowing for a systematic investigation of tracer diffusion over a previously unexplored range of loading. These studies showed that (1) the normalized diffusion coefficients collapsed onto a master curve when plotted versus the confinement parameter defined as the interparticle distance divided by the tracer size ($ID/2R_g$), (2) the normalized diffusion coefficients decreased more rapidly for ID values smaller than ~$2R_g$, suggesting a second mechanism for slowing down at high confinement, and (3) diffusion was reduced by 80% at 50 vol %. In a follow-up study,[27] tracer diffusion was studied in the same weakly interacting polymer−NP system to evaluate the effect of NP diameter, 13 and 29 nm, and NP polydispersity. The normalized diffusion coefficients collapsed onto a master curve at the two NP sizes. The effect of polydispersity, although minor, was found to bring results into better agreement for the more polydisperse small NPs. These findings validate using the confinement parameter (ranging from 0.1 to 3) to produce a master curve for weak polymer−NP interactions.

Using molecular dynamics simulations, Kumar et al.[28] showed that polymer diffusion slowed down if nanoparticles are attracted to the diffusing polymer. Experiments by Hu et al.[29] found that the diffusion coefficients of poly(methyl methacrylate), dPMMA, decreased by a factor of 3 as clay concentration increased to 5 vol % in PMMA matrix, whereas slowing down was not observed in a nonattractive matrix of PS and clay.

In the present study, we probe tracer diffusion in a polymer composite having attractive interactions between spherical nanoparticles and the tracer (matrix) chains. The polymer nanocomposite contains a PMMA matrix mixed with hydroxyl-functionalized silica nanoparticles with diameters of 12.8, 28.8, and 49.3 nm, denoted as NP13, NP29, and NP50, respectively. Because of the attractive interaction between PMMA and silica, the NPs are well dispersed at volume fractions ranging from 0.05 to 50 vol %. The tracer diffusion of dPMMA in PMMA/silica can be compared with prior studies in a weakly interacting system and thereby allow new insights about the role of interactions on polymer dynamics in PNCs. For the tracer diffusion of dPMMA in PMMA/silica, the normalized diffusion coefficients collapse on a master curve where diffusion occurs in highly confined ($ID < 2R_g$) and weakly confined ($ID > 2R_g$) regions. Furthermore, the normalized diffusion coefficients for the weakly interacting system[26] are in good agreement with this master curve, suggesting that interactions between polymer and nanoparticles do not significantly affect center-of-mass diffusion.

EXPERIMENTAL SECTION

Materials. Poly(methyl methacrylate) (PMMA) (MW = 337 000 g mol^{-1}, polydispersity (PDI) = 1.82; MW = 600 000 g mol^{-1}, PDI = 3.3, Sigma-Aldrich) and deuterated PMMA (dPMMA) (MW = 100 000 g mol^{-1}, PDI = 1.06) were used as received. Molecular weight and PDI were determined by size exclusion chromatography (SEC) using tetrahydrofuran (THF) as the solvent. Three different nanoparticles were used in this work, and they are referred as NP13, NP29, and NP50. The number-average diameter (d_n) and the size polydispersity (σ) are summarized in Table 1. NP13 (Nissan Chemical) and NP29 (Ludox) were used as received. NP50 (Nissan Chemical) was solvent transferred from isopropanol (IPA) to *N*,*N*-dimethylacetamide (DMAC). d_n and σ were determined using small-angle X-ray scattering (SAXS) and dynamic light scattering (DLS) with log-normal distribution fitting[30]

Table 1. Silica Nanoparticle Characteristics: Number-Average Diameter and Size Polydispersity

name	d_n (nm)	σ^a
NP13	12.8	1.39
NP29	28.8	1.13
NP50	49.3	1.30

[a] σ is defined using the log-normal distribution, eq 1.

$$f(d_i) = \frac{e^{-((\ln d_i - \ln d_m)^2/2(\ln \sigma)^2}}{(\ln \sigma)^2\sqrt{2\pi}} \quad (1)$$

where $f(d_i)$ is the probability of finding a particle having diameter d_i, d_m is the geometric mean diameter, and σ is NP size polydispersity. Figure 1 shows the size distribution of NP13, NP29, and NP50. NP29 has the smallest σ and thus has the narrowest distribution. As the size of the

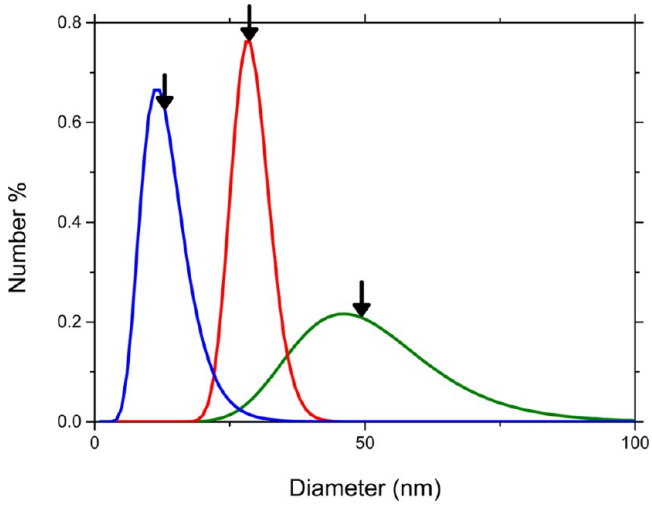

Figure 1. Size distribution for NP13 (blue curve), NP29 (red curve), and NP50 (green curve) as determined from DLS. Arrows denote the number-average diameters 12.8, 28.8, and 49.3 nm, respectively. Using a log-normal distribution, the polydispersities are 1.39, 1.13, and 1.30, respectively.

dx.doi.org/10.1021/ma4000557 | Macromolecules 2013, 46, 4502−4509

particle increases, the distribution could be wider at fixed σ. For example, the distribution of NP50 is across a wider range than that of NP13 observed in Figure 1 although its σ is similar to the σ of NP13.

Zeta potentials (ζ) of NP13, NP29, and NP50 are -38.7 ± 3, -38 ± 6, and -88.6 ± 3 mV, respectively, determined by a Delsa Nano C particle analyzer.

Preparation and Characterization of Polymer Nanocomposites. In this work, a polymer nanocomposite was composed of PMMA and silica NPs. We aimed to well-disperse the silica nanoparticles in the PMMA matrix. PMMA was dissolved in dimethylacetamide (DMAC) or dimethylformamide (DMF) and was stirred for 20 h. Nanoparticles were dispersed in DMAC. The nanoparticle solution was sonicated overnight before being mixed with the PMMA solution. An appropriate amount of the nanoparticle solution was mixed with the PMMA solution. Films were prepared by doctor blading the mixed solution on a heated (150 °C) glass substrate, which allows the solvent to evaporate rapidly. After doctor blading, the film was dried at 150 °C in a hood for 30 min and then was dried under vacuum at 150 °C for 24 h. The resulting thickness of the film was about 5 μm as determined by ellipsometry. The nanoparticle volume fractions were determined using thermal gravimetric analysis (TGA). The films were heated at 10 °C/min from 20 to 400 °C and held at 400 °C for 2 h. The NP volume fractions for each nanocomposites are summarized in Table 2. The type of the nanocomposite is named as PMMA/NPx, where x is 13, 29, and 50. The distribution of the nanoparticles were observed using TEM after cross-sectioning the nanocomposite thin film using a microtome. Small-angle X-ray scattering (SAXS) was also used to observe the distribution of the nanoparticles in the PMMA/NP29 nanocomposite.[31] Glass transition temperatures were determined using differential scanning calorimetry (DSC). The nanocomposite films (~8 mg) were placed in an aluminum pan and heated from 20 to 160 °C at 10 °C/min.

Table 2. PMMA/Silica Nanocomposites

nanocomposite	NP volume fraction				
PMMA/NP13	0.005	0.035	0.07	0.14	0.25
PMMA/NP29	0.01	0.05	0.10	0.20	0.40
PMMA/NP50	0.02	0.05	0.15	0.25	0.40

Diffusion Couple Preparation and Annealing. The diffusion couple consisted of a thick (~5 μm) nanocomposite film covered with a layer of thin dPMMA film. The nanocomposite film was floated from the glass substrate in water and picked up using a silicon wafer. The nanocomposite film on the wafer was aged at 150 °C for 3 days in vacuo. The dPMMA tracer film was spin-coated on a silicon wafer and had a thickness ~20 nm as measured by ellipsometry. The tracer film was transferred from the silicon wafer to the top of the nanocomposite film, forming a diffusion couple. The diffusion couple was dried under ambient conditions overnight and then annealed isothermally at 195 °C under a nitrogen purge on a Metler hot plate. The annealing time was chosen to allow sufficient penetration of the dPMMA into the matrix, typically ~300 nm. To ensure consistency of annealing condition, a control sample of dPMMA/PMMA was annealed adjacent to the sample.

Elastic Recoil Detection (ERD). ERD was used to probe the dPMMA depth profile in the nanocomposite. Details of ERD have been reviewed elsewhere.[32] The measurement was conducted under room temperature. The energy of the incident helium ion (He^{2+}) beam was ~3.022 MeV, and the ion beam intersected the plane of the sample at 15°. The energy of the recoiled atom was detected by a solid-state detector. A 10 μm Mylar film was placed in front of the detector in order to filter forward scattered helium that masked the hydrogen and deuterium signal. A low beam current (<2 nA) was used, and a total 10 μC was collected from five different spots on the diffusion couple sample. The ERD spectra of count versus channel were converted to dPMMA depth profile of dPMMA volume fraction versus depth. The diffusion coefficient of the tracer was obtained by

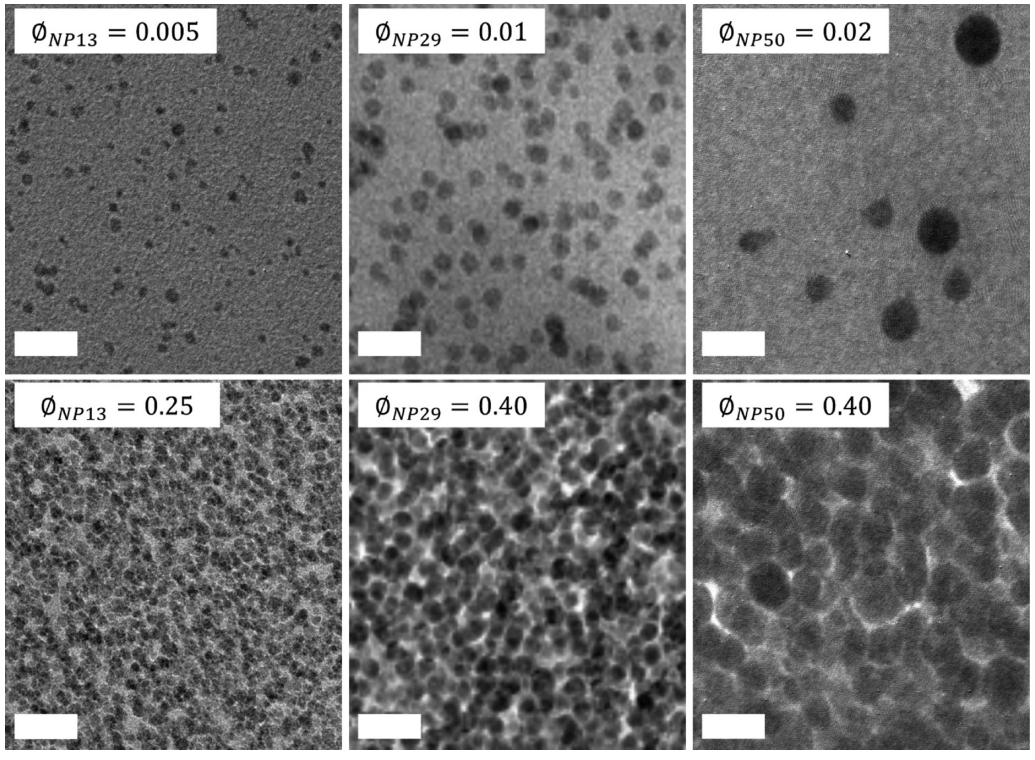

Figure 2. Cross-sectional TEM images of PMMA matrices containing NP13, NP29, and NP50. Individual NPs are observed at the lowest volume fractions prepared (top row). At the highest volume fractions (bottom row), the NP distribution remains uniform. The interparticle distance (ID) is much greater than the NP diameter in the top row, whereas $ID \ll$ NP diameter in the bottom row for the crowded composite (cf. Figure 5). The scale bars are 100 nm.

dx.doi.org/10.1021/ma4000557 | Macromolecules 2013, 46, 4502−4509

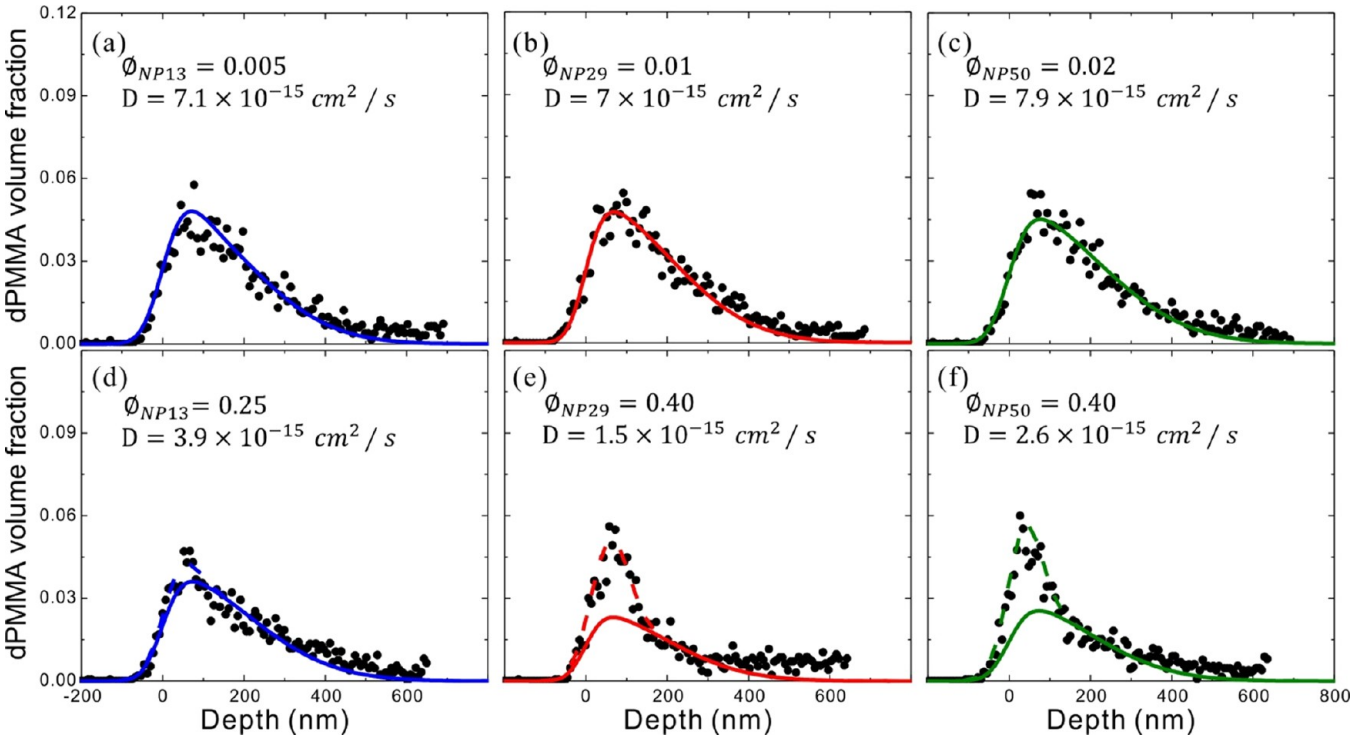

Figure 3. Volume fraction profiles of dPMMA in PMMA/NP13 (a, d), PMMA/NP29 (b, e), and PMMA/NP50 (c, f) at 195 °C. (a–c) and (d–f) correspond to the lowest and highest values of ϕ_{NP}, respectively. Solid curves represent fits using eq 2 convoluted with a Gaussian instrumental resolution function. In (e) and (f) the dashed curves represent the sum of the solid curves and surface peaks. Annealing times of (a) 7.8, (b) 7.95, (c) 7.95, (d) 15, (e) 33.37, and (f) 20 h were chosen to provide an optimum diffusion length ~350 nm.

fitting the depth profile using the one-dimensional (1-D) solution of Fick's second law for a finite source in a semi-infinite medium.[33] The instrumental resolution (σ), or half of the full width at half-maximum (fwhm), was captured by the Gaussian function $y = [1/\sigma(2\pi)^{1/2}] \exp(-x^2/2\sigma^2)$, where y is the dPMMA fraction and x is the depth. σ is 40 nm, and the accessible depth was ~800 nm. The diffusion coefficients obtained in this work were from multiple measurements. Only the depth profiles having a sufficient diffusion length (>200 nm) were used.

RESULTS AND DISCUSSION

Distribution of Nanoparticles in Polymer Nanocomposites. Before investigating polymer dynamics, the distribution of nanoparticles is studied. A good dispersion is required because nanoparticle aggregation results in an effective larger interparticle distance, which can increase polymer mobility. The cross-sectional TEM images shown in Figure 2 demonstrate that silica nanoparticles disperse in the PMMA matrix without aggregating. At low nanoparticle loadings (top row), individual NPs are observed. The volume fraction was increased from 0.5 to 2 vol % to partially compensate for the decrease in number density as NP size increases. At high NP loading (bottom row), the NPs are also well dispersed and the interparticle distance is on the length scale of R_g. Qualitatively, a comparison of the NP29 and NP50 at 40 vol % shows that the number density decreases as the NP size increases, as expected. Theoretically, the number density should be about 5 times larger for the NP29 system. Because the image represents a ~100 nm thick cross section of the film an accurate measure of distance and number density is challenging via TEM. Using SAXS and TEM, Meth et al.[31] showed that the distribution of NP29 in a PMMA matrix prepared by the same method are well dispersed, in agreement with Figure 2 (center column). The effect of size polydispersity is also apparent at low loading. Namely, NP29 particles have very similar diameter consistent with its low polydispersity. Although having a similar polydispersity, NP50 appears to exhibit a larger range of diameters than NP13, likely because of the low number (~8) of imaged particles. Thus, these TEM results are in qualitative agreement with the polydispersities for NP13, NP29, and NP50 measured by DLS and shown in Figure 1.

In contrast to the polystyrene/phenyl-capped silica previously investigated, silica nanoparticles with surface hydroxyl groups (i.e., colloidal silica) have an attractive interaction with PMMA, and this affinity drives the dispersion because PMMA chains preferentially wet silica. By studying adsorption from trichloroethylene, Kawaguchi et al.[34] showed that PMMA strongly adsorbs to silica which prevents nanoparticles from aggregating. In the present studies, the high molecular weight of the PMMA matrix provides a highly viscous environment for the nanoparticles at low solvent concentrations, further preventing aggregation during the casting of matrix films.[31] In summary, the TEM studies show that the NP13, NP29, and NP50 are well-dispersed in PMMA across a wide range of volume fractions, and therefore the PMMA:silica matrix provides a stable structure for subsequent diffusion studies.

Tracer Diffusion in Nanocomposites. Using ERD, the tracer diffusion coefficients of dPMMA (100 kg/mol) in PMMA/NPx were determined as a function of the nanoparticle size (d_n) and volume fraction (ϕ_{NP}). The dPMMA volume fraction profile was obtained after annealing the diffusion couple. This profile can be described by the 1-D solution to Fick's second law for a finite source in a semi-infinite medium. The deuterated volume fraction, $\phi(x)$, is given by[33]

dx.doi.org/10.1021/ma4000557 | Macromolecules 2013, 46, 4502–4509

$$\phi(x) = \frac{1}{2}\left[\mathrm{erf}\left(\frac{h-x}{\sqrt{4Dt}}\right) + \mathrm{erf}\left(\frac{h+x}{\sqrt{4Dt}}\right)\right] \quad (2)$$

where x is depth, h is original dPMMA film thickness, t is diffusion time, and D is the diffusion coefficient of dPMMA. An experimental depth profile was fitted by $\phi(x)$ convoluted with the Gaussian instrumental resolution function. Quality fits were obtained by minimizing χ^2 using least-squares fitting. Figure 3 shows representative depth profiles (solid circles) and their fits (solid lines) for dPMMA diffusion into (a, d) PMMA/NP13, (b, e) PMMA/NP29, and (c, f) PMMA/NP50 at the lowest (top row) and the highest (bottom row) volume fractions of nanoparticles. The depth profiles follow Fickian diffusion, eq 2, at low volume fractions. At high volume fractions, surface peaks are observed for tracer diffusion. As previously described,[26] this surface peak is attributed to an initial reduction in flux at the interface between the tracer layer and the nanocomposite due to the impenetrable silica nanoparticles. A Gaussian function was used to fit the surface peak and then added to the Fickian diffusion profiles (dashed lines in e and f). Consistent with our prior study,[26] the magnitude of the peak decays with time as more of the dPMMA is able to penetrate into the matrix. For dPMMA diffusion into PMMA/NP13, PMMA/NP29, and PMMA/NP50, the tracer diffusion coefficients decrease by more than a factor of 2 as NP loading increases from its minimum to maximum values. This demonstrates that nanoparticles slow down center-of-mass diffusion of dPMMA in PMMA/silica nanoparticle systems. Before addressing the key question about the role of interfacial interactions, we first address the issue of the glass transition.

Diffusion coefficients are very sensitive to temperature, so it is most appropriate to compare D at fixed $T - T_g$, where T is the annealing temperature and T_g is the glass transition temperature of the composites. The glass transition temperatures of the PMMA/NPx matrices are summarized in Table 3.

Table 3. Summary of the T_g Changes for Different Nanoparticle Volume Fractions in NP13, NP29, and NP50 Nanocomposites; Values of the Zeta Potential (ζ) of Nanoparticles in DMAC Are in the Far Right Column[a]

ϕ_{NP13}	0.005	0.07	0.14	0.25		ζ (mV)
ΔT_g (°C)	−1	−0.1	−0.8	−0.1		−38.7 ± 3
ϕ_{NP29}	0.01	0.05	0.10	0.20	0.40	ζ (mV)
ΔT_g (°C)	−1	−0.3	−0.8	0.1	1.7	−38 ± 6
ϕ_{NP50}	0.02	0.05	0.15	0.25	0.40	ζ (mV)
ΔT_g (°C)	0.65	−0.25	1.4	4	4.65	−88.6 ± 3

[a] $\Delta T_g = T_{g,PMMA/NPx} - T_{g,PMMA}$, where $T_{g,PMMA}$ = 120 °C.

Whereas the T_g's of PMMA/NP13 and PMMA/NP29 are relatively constant, the T_g of PMMA/NP50 increases at high volume fractions. At ϕ_{NP} = 0.40 in PMMA/NP50, the T_g is 4.6 K higher than that of the pure PMMA matrix. This increase in the glass transition temperature is attributed to the attractive interaction between the hydroxyl-capped surface of silica and PMMA. For a PMMA/silica nanocomposite containing 62.5 wt % silica, Moll et al.[19] observed a T_g increase of ~7 K, in good agreement with our findings. The question then becomes why the glass transition temperature increases for PMMA/NP50 but remains nearly constant for the PMMA/NP13 and PMMA/NP29 matrices. Because T_g depends on the interaction between surface groups on the NP and the surrounding polymer, the surfaces of NP13, NP29, and NP50 may contain different areal densities of hydroxyl groups. To test this hypothesis, the zeta potentials (ζ) of NP13, NP29, and NP50 were determined in DMAC, the same solvent used to cast the PMMA/NPx nanocomposite films. The ζ of NP13 and NP29 are similar, whereas the ζ of NP50 is twice that of NP13 and NP29, as summarized in Table 1. Because the ζ reflects the surface charge,[35] NP50 has a higher concentration of hydroxyl groups, which in turn allows for more attractive interactions with PMMA segments and a corresponding increase in T_g. Thus, even within the PMMA/silica NP system, we have a range of interfacial attractions. To account for the higher glass transition temperature in the PMMA/NP50 matrices, the diffusion coefficients were shifted using the Williams−Landel−Ferry (WLF) equation:[36]

$$\log\left(\frac{D(T_0)}{D(T_1)}\right) = \frac{-C_1(T - T_0)}{C_2 + T - T_0} \quad (3)$$

where T_0 is the reference temperature, here the glass transition temperature, 393 K, is used, T_1 is the shifted temperature, T is the annealing temperature, C_1 = 11.9, and C_2 = 69 K.[37] Thus, all values are compared at $T - T_g$ = 75 K, where T_g is the glass transition temperature of the nanocomposite. For example, for the PMMA/NP50 system with ϕ_{NP} = 0.40, the diffusion coefficient should be determined at 199.6 °C to account for the 4.6 °C increase in T_g. By comparing at $T - T_g$ = constant, differences in the diffusion coefficient of dPMMA can be attributed to the NP volume fraction, NP size, and NP spacing.

The normalized diffusion coefficients (D/D_0) are plotted against the nanoparticle volume fraction in Figure 4. At low

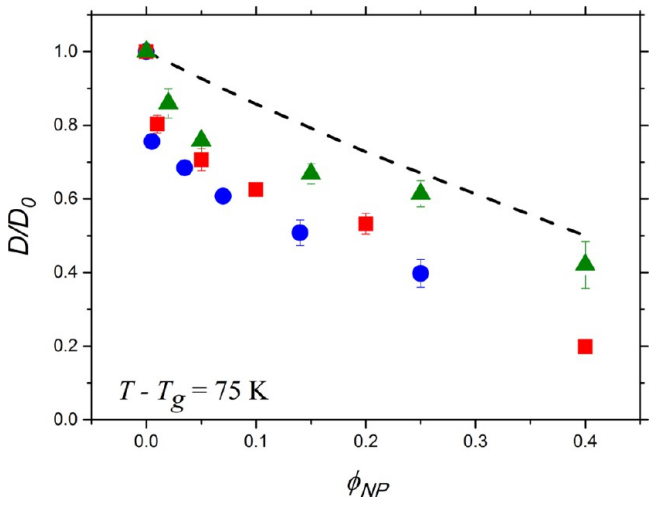

Figure 4. Normalized diffusion coefficients versus NP volume fraction for dPMMA diffusion in PMMA/NP50 (green triangles), PMMA/NP29 (red squares), and PMMA/NP13 (blue circles). The black dotted line is the calculation from the Maxwell model.

nanoparticle loading, the diffusion coefficient decreases sharply as loading increases. For example, the diffusion coefficient decreases ~25% upon adding only 0.005 of NP13 to the PMMA matrix. The diffusion coefficient continues to decrease, although less sharply, at high NP loadings. Plotting D/D_0 at a fixed $(T - T_g)$ as a function of nanoparticle volume fraction does not collapse the three sets of date representing the PMMA/NP13, PMMA/NP29, and PMMA/NP50 matrices. Namely, compared at the same volume fraction, the diffusion

dx.doi.org/10.1021/ma4000557 | Macromolecules 2013, 46, 4502−4509

coefficient decreases as the NP size decreases from 50 to 29 to 13 nm. This result may be attributed to the increase in the number of obstacles to diffusion as size decreases. However, when plotted versus the number density of NPs, D/D_0 does not collapse on a master curve (as shown in Supporting Information Figure S1). As a reference, we include the prediction of the Maxwell model,[38] showing, as in our previous studies, that tortuosity along does not account for the slowing down of diffusion in the presence of immobile silica nanoparticles.

Confinement Parameter. For diffusion into a system with weak polymer−NP interactions, the normalized diffusion coefficient was shown to collapse on a master curve when plotted against the confinement parameter.[26] The confinement parameter is defined as the ratio of the interparticle distance (ID) relative to the probe size, $2R_g$, where R_g is the radius of gyration of the dPMMA tracer chain. Thus, $ID/2R_g$ represents the melt region available for polymer chains to diffuse between a fixed array of randomly placed nanoparticles.

Given that the nanoparticles are well-dispersed in the PMMA matrix, ID in 3D can be calculated[27,39] under the assumption that nanoparticles are randomly distributed:

$$ID = d_n\left[\left(\frac{2}{\phi_{NP}\pi}\right)^{1/3} e^{\ln \sigma^2} - 1\right] \quad (4)$$

Thus, ID depends on nanoparticle size (d_n), nanoparticle volume fraction (ϕ_{NP}), and nanoparticle size polydispersity (σ). Figure 5 shows how ID decreases as the nanoparticle volume

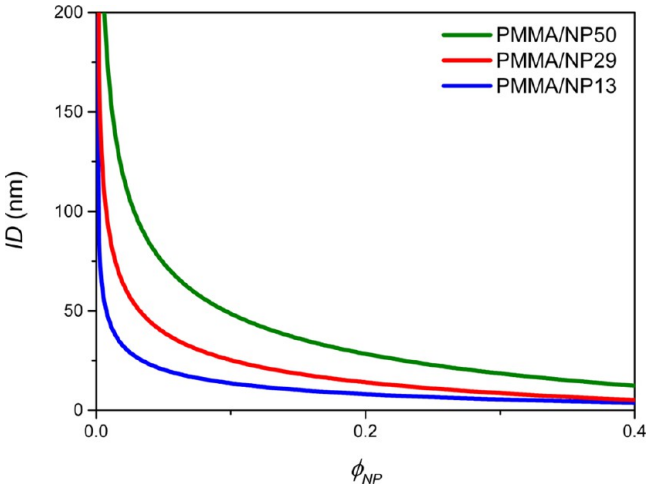

Figure 5. Average interparticle distance (ID) as a function of nanoparticle volume fraction (ϕ_{NP}) using eq 4, which assumes randomly distributed NPs. ID decreases rapidly at low nanoparticles loadings. At fixed ϕ_{NP}, ID decreases as NP size decreases when compared at the same ϕ_{NP}.

fraction increases up to 0.40. For NP13, NP29, and NP50, ID drops dramatically at low ϕ_{NP}; for NP13, ID decreases by ∼150 nm when ϕ_{NP} increases from 0 to 0.01. In contrast, ID decreases relatively weakly at higher ϕ_{NP} (i.e., ϕ_{NP} > ∼0.1; for NP13, ID decreases by only 13 nm as ϕ_{NP} increases from 0.05 to 0.25.) Furthermore, at the same ϕ_{NP}, ID increases as the nanoparticle diameter increases. For example, at 10 vol %, the ID of PMMA/NP50 is 43.6 nm, which is more than 3 times larger than the ID value in the PMMA/NP13, 13.6 nm. This difference reflects the lower number density of NP50.

The probe size is described by the radius of gyration (R_g) of dPMMA, assuming that chains obey Gaussian statistics, and given by[40]

$$R_g = \frac{a\sqrt{N}}{\sqrt{6}} = \frac{a\sqrt{M_w/M_0}}{\sqrt{6}} \quad (5)$$

where a is the monomer length (0.66 nm), N is the degree of polymerization, M_w is the weight-averaged molecular weight, and M_0 is the molar mass of a monomer unit (108.12 g/mol). For M_w = 100 kg/mol, R_g = 8.2 nm.

When the confinement parameter is greater than 1, the diffusion of dPMMA between the immobile particles is reduced. However, when the confinement parameter is less than 1, the dPMMA chain is larger than the average space between particles. In this crowded regime, either the tracer must be patient, probe its surroundings and find a path between particles with a large spacing, or suffer the loss of configurational entropy by squeezing between closely spaced particles. The competition between the former case, which corresponds to a limited number of broad pathways, and the latter case, which corresponds to the greater number of narrow pathways, is likely to dictate the magnitude of diffusion. At present, there are no models that relate the materials parameters ϕ_{NP}, d_n, and ID to the tracer diffusion coefficient in a polymer nanocomposite.

Figure 6 shows that the normalized diffusion coefficients fall on a master curve when plotted against the confinement

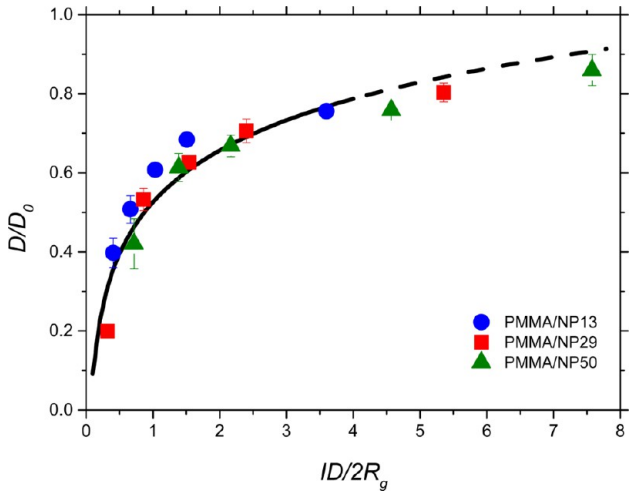

Figure 6. Normalized diffusion coefficients (D/D_0) plotted against the confinement parameter ($ID/2R_g$). Data points represent D/D_0 in the attractive system (PMMA/hydroxyl-capped silica): PMMA/NP13 (blue circle), PMMA/NP29 (red square), and PMMA/NP50 (green triangle). The solid black line is the best fit to the weakly interacting system (PS/phenyl-capped silica) from a previous study.[26] The dashed line shows that the extrapolation of the weakly interacting system is also in good agreement with the measured values at higher $ID/2R_g$ for the strongly interacting system.

parameter for the PMMA/NP13, PMMA/NP29, and PMMA/NP50 systems. Whereas prior studies investigated confinement parameters up to ∼3,[26,27] the present system extends this range out to $ID/2R_g$ ∼ 8. These studies show that even when the spacing between nanoparticles is about 8 times greater than the size of the tracer molecule the diffusion coefficient is reduced by 15%. Similar to prior studies,[26] as the confinement parameter decreases, D/D_0 decreases weakly as $ID/2R_g$ varies

dx.doi.org/10.1021/ma4000557 | Macromolecules 2013, 46, 4502−4509

from ∼8 to ∼2. However, for $ID/2R_g$ < ∼2, D/D_0 decreases very strongly with a much steeper slope than at low $ID/2R_g$. In this highly confined regime, for example, at $ID/2R_g \sim 0.4$, the diffusion coefficient is reduced by 80%.

The empirical relationship between D/D_0 and $ID/2R_g$ indicates that the center-of-mass diffusion of macromolecules slows down as the particle spacing relative to the tracer chain size decreases. However, the mechanism of this slowing down is not well understood. According to a modified reptation model proposed by Richter et al.,[41] the local dynamics of polymer chains are not altered by the presence of NPs, but rather add to the physical constraints due to entanglements resulting in a reduced entanglement density. Thus, the additional geometric constraint provided by the nanoparticles reduces the apparent tube diameter and thus slows down polymer dynamics. This model seemed to capture the dynamics of poly(ethylene-*alt*-propylene) containing hydrophobically modified silica (diameter = 17 nm). Using PRISM theory, Yamamoto and Schweizer[42] showed that the addition of nanoparticles changes how polymer chains can pack in a nanocomposite, altering the friction in the melt. In addition, Harton et al.[17] found nanoparticles with a favorable attraction toward the polymer results in an immobilized layer around the nanoparticles. This immobilized layer exhibits slower segmental motion, and thus larger friction, a possible explanation for the slowing down of tracer diffusion.

To determine if attractive interactions between PMMA and silica NPs slow down diffusion, we compare the dPMMA tracer diffusion studies in Figure 6 with results from our previous study[26] of deuterated polystyrene (dPS) diffusing into a matrix of PS and phenyl-capped silica, which is the same core particle as NP29 in the present study. Because PS only weakly interacts with the hydrophobic silica, the diffusion of dPS would be faster relative to the PMMA/NPx studies if attractions slow down diffusion. However, as seen in Figure 6, D/D_0 for the PS/NP29 system (solid curve) is very similar to the PMMA/NPx case (symbols), particularly for $ID/2R_g$ > ∼2. In the highly confined regime, the PS data fall slightly above the PMMA results, indicating slower diffusion. Because the PS studies were performed at 145 to 170 °C and scaled to $T - T_g$ = 66 °C, systematic studies of the temperature dependence of diffusion are needed before further comment about this small difference with the PMMA/NPx results, measured at 195 °C and scaled to $T - T_g$ = 75 K, can be made. Whereas the T_g of PMMA/NP50 increased at high NP loading, the T_g for the PS nanocomposites remained constant. Thus, although attractive interactions can affect local relaxations, these favorable interactions do not appear to slow down macroscopic diffusion. One possible explanation is that each new interaction between a dPMMA segment and silica is offset by a loss of a PMMA segment/silica interaction, resulting in no net enthalpic change. To address the possibility that the PMMA matrix chains form an immobilized layer that masks the interaction between dPMMA and silanol groups on the NPs, we performed the following experiment. A tracer film of dPMMA/NP13 (1 vol %) was deposited over a PMMA matrix. For comparison, a control bilayer of dPMMA:PMMA was prepared. After annealing for 9.5 h, at 195 °C, the volume fraction profiles of dPMMA from the nanocomposite tracer and pure tracer were compared and found to overlap. These experiments indicate that the exchange between matrix PMMA and dPMMA adjacent to the NPs occurs on the time scale of these diffusion studies. Regardless of the reason, our experimental studies demonstrate that diffusion in polymer nanocomposites having weak and attractive interactions can both be described by a confinement parameter that reflects the spacing between nanoparticles, which depends on volume fraction and diameter, relative to the tracer size.

■ CONCLUSION

In this study, we present the first systematic experimental studies of tracer diffusion in a polymer nanocomposite having attractive interactions. Macromolecular diffusion in polymer nanocomposites having a strong segment/nanoparticle interaction is probed by tracer diffusion using ERD. Nanoparticles are uniformly dispersed in PMMA matrix, even up to very high loadings, ϕ_{NP} = 0.4 for PMMA/NP29 and PMMA/NP50, such that these nanocomposites are ideal matrices for tracer diffusion studies. The glass transition temperature for PMMA/NP50 is found to increase by ∼5 K, consistent with the literature. The enhancement of T_g is attributed to the high surface charge of NP50 resulting in strong segmental/nanoparticle attraction (higher surface potential). Upon comparing at the same $T - T_g$, the normalized diffusion coefficients decrease as ϕ_{NP} increases, implying that nanoparticles hinder center-of-mass diffusion. This slowing down increases as the size of the NP decreases (i.e., compared at same ϕ_{NP}).

The confinement parameter, $ID/2R_g$, which captured the effect of ϕ_{NP} and NP size on diffusion in a weakly interacting system, is tested for a strongly interacting system. When D/D_0 is plotted against the confinement parameter, all data collapse onto a master curve, suggesting that the confinement parameter is able to capture the effect of ϕ_{NP} and NP size on the diffusion even for systems with attractive or weak interactions. For $ID/2R_g$ between ∼8 and ∼2, the diffusion coefficients decrease slowly as $ID/2R_g$ decreases. For example, the diffusion coefficient is found to decrease by 15% even when ID is much larger than the probe size, $2R_g$, by a factor of 8. This result shows that the presence of even very dilute concentrations of NPs have a large effect on polymer dynamics. For $ID/2R_g$ < ∼2, the diffusion coefficients decrease sharply as ϕ_{NP} decreases. For example, the diffusion coefficient decreases by 80% at $ID/2R_g$ = 0.25.

Furthermore, the tracer diffusion of dPMMA in PMMA/NP*x* is compared to prior studies in the weakly interacting polymer nanocomposite and found to be in reasonable agreement. Namely, the reduced diffusion coefficients from both systems nearly collapse on the same master curve, suggesting that the confinement parameter captures slowing down independent of segment/nanoparticle interactions. At present, the mechanism of polymer diffusion in the presence of immobile, impenetrable nanoparticles is lacking. Clearly, any theory would need to capture the behavior in the confined regime ($ID/2R_g$ > ∼2) and highly confined regime where nanoparticle spacing, on average, is less than the size of the tracer. These studies, combined with prior ones on weakly interacting systems, provide guidance for testing future models and theories describing polymer dynamics in polymer nanocomposites with immobile, impenetrable nanoparticles.

■ ASSOCIATED CONTENT

Supporting Information

Figure S1. This material is available free of charge via the Internet at http://pubs.acs.org.

dx.doi.org/10.1021/ma4000557 | *Macromolecules* 2013, 46, 4502−4509

AUTHOR INFORMATION

Corresponding Author

*E-mail: composto@seas.upenn.edu (R.J.C.).

Notes

The authors declare no competing financial interest.

ACKNOWLEDGMENTS

This research was funded primarily by the National Science Foundation NSF/EPSRC Materials World Network DMR-0908449. Support was also provided by the NSF/MRSEC-DMR 11-20901 (K.I.W., R.J.C.) and Polymer Programs DMR 09-07493 (R.J.C.) as well as the EP/G065373/1 (N.C.). We thank Prof. Schweizer for useful discussions. We also thank Central Research and Development, DuPont Co., for generous support.

REFERENCES

(1) Gilman, J. W. *Appl. Clay Sci.* **1999**, *15* (1−2), 31−49.
(2) Park, J. H.; Jana, S. C. *Polymer* **2003**, *44* (7), 2091−2100.
(3) Hore, M. J. A.; Frischknecht, A. L.; Composto, R. J. *ACS Macro Lett.* **2012**, *1* (1), 115−121.
(4) White, S. I.; Mutiso, R. M.; Vora, P. M.; Jahnke, D.; Hsu, S.; Kikkawa, J. M.; Li, J.; Fischer, J. E.; Winey, K. I. *Adv. Funct. Mater.* **2010**, *20* (16), 2709−2716.
(5) Winey, K. I.; Vaia, R. A. *MRS Bull.* **2007**, *32* (4), 314−319.
(6) Jancar, J.; Douglas, J. F.; Starr, F. W.; Kumar, S. K.; Cassagnau, P.; Lesser, A. J.; Sternstein, S. S.; Buehler, M. J. *Polymer* **2010**, *51* (15), 3321−3343.
(7) Tuteja, A.; Mackay, M. E.; Hawker, C. J.; Van Horn, B. *Macromolecules* **2005**, *38* (19), 8000−8011.
(8) Tuteja, A.; Duxbury, P. M.; Mackay, M. E. *Macromolecules* **2007**, *40* (26), 9427−9434.
(9) Doi, M.; Edwards, S. F. *The Theory of Polymer Dynamics*; Clarendon: Oxford, 1986.
(10) Bogoslovov, R. B.; Roland, C. M.; Ellis, A. R.; Randall, A. M.; Robertson, C. G. *Macromolecules* **2008**, *41* (4), 1289−1296.
(11) Rittigstein, P.; Priestley, R. D.; Broadbelt, L. J.; Torkelson, J. M. *Nat. Mater.* **2007**, *6* (4), 278−282.
(12) Ellison, C. J.; Torkelson, J. M. *Nat. Mater.* **2003**, *2* (10), 695−700.
(13) Blum, F. D.; Young, E. N.; Smith, G.; Sitton, O. C. *Langmuir* **2006**, *22* (10), 4741−4744.
(14) vanZanten, J. H.; Wallace, W. E.; Wu, W. L. *Phys. Rev. E* **1996**, *53* (3), R2053−R2056.
(15) Park, C. H.; Kim, J. H.; Ree, M.; Sohn, B. H.; Jung, J. C.; Zin, W. C. *Polymer* **2004**, *45* (13), 4507−4513.
(16) Sargsyan, A.; Tonoyan, A.; Davtyan, S.; Schick, C. *Eur. Polym. J.* **2007**, *43* (8), 3113−3127.
(17) Harton, S. E.; Kumar, S. K.; Yang, H.; Koga, T.; Hicks, K.; Lee, E.; Mijovic, J.; Liu, M.; Vallery, R. S.; Gidley, D. W. *Macromolecules* **2010**, *43* (7), 3415−3421.
(18) Brown, D.; Marcadon, V.; Mele, P.; Alberola, N. D. *Macromolecules* **2008**, *41* (4), 1499−1511.
(19) Moll, J.; Kumar, S. K. *Macromolecules* **2012**, *45* (2), 1131−1135.
(20) Degennes, P. G. *J. Chem. Phys.* **1971**, *55* (2), 572.
(21) Riggleman, R. A.; Toepperwein, G.; Papakonstantopoulos, G. J.; Barrat, J. L.; de Pablo, J. J. *J. Chem. Phys.* **2009**, *130* (24), 244903.
(22) Martin, J.; Krutyeva, M.; Monkenbusch, M.; Arbe, A.; Allgaier, J.; Radulescu, A.; Falus, P.; Maiz, J.; Mijangos, C.; Colmenero, J.; Richter, D. *Phys. Rev. Lett.* **2010**, *104* (19), 197801.
(23) Nusser, K.; Schneider, G. J.; Pyckhout-Hintzen, W.; Richter, D. *Macromolecules* **2011**, *44* (19), 7820−7830.
(24) Mackay, M. E.; Dao, T. T.; Tuteja, A.; Ho, D. L.; Van Horn, B.; Kim, H. C.; Hawker, C. J. *Nat. Mater.* **2003**, *2* (11), 762−766.
(25) Anderson, B. J.; Zukoski, C. F. *Macromolecules* **2009**, *42* (21), 8370−8384.
(26) Gam, S.; Meth, J. S.; Zane, S. G.; Chi, C.; Wood, B. A.; Seitz, M. E.; Winey, K. I.; Clarke, N.; Composto, R. J. *Macromolecules* **2011**, *44* (9), 3494−3501.
(27) Gam, S.; Meth, J. S.; Zane, S. G.; Chi, C.; Wood, B. A.; Winey, K. I.; Clarke, N.; Composto, R. J. *Soft Matter* **2012**, *8* (24), 2512−2520.
(28) Desai, T.; Keblinski, P.; Kumar, S. K. *J. Chem. Phys.* **2005**, *122*, 13.
(29) Hu, X. S.; Zhang, W. H.; Si, M. Y.; Gelfer, M.; Hsiao, B.; Rafailovich, M.; Sokolov, J.; Zaitsev, V.; Schwarz, S. *Macromolecules* **2003**, *36* (3), 823−829.
(30) Irani, R. R. *Particle Size: Measurement, Interpretation and Application*; Wiley: New York, 1963.
(31) Meth, J. S.; Zane, S. G.; Chi, C.; Londono, J. D.; Wood, B. A.; Cotts, P.; Keating, M.; Guise, W.; Weigand, S. *Macromolecules* **2011**, *44* (20), 8301−8313.
(32) Composto, R. J.; Walters, R. M.; Genzer, J. *Mater. Sci. Eng., R* **2002**, *38* (3−4), 107−180.
(33) Crank, J. *The Mathematics of Diffusion*, 2nd ed.; Clarendon Press: Oxford, 1975; p 414.
(34) Kawaguchi, M.; Yamagiwa, S.; Takahashi, A.; Kato, T. *J. Chem. Soc., Faraday Trans.* **1990**, *86* (9), 1383−1387.
(35) Israelachvili, J. N. *Intermolecular and Surface Forces: With Applications to Colloidal and Biological Systems*; Academic Press: London, 1985.
(36) Ferry, J. D. *Viscoelastic Properties of Polymers*; Wiley: New York, 1980.
(37) Colby, R. H. *Polymer* **1989**, *30* (7), 1275−1278.
(38) Maxwell, C. *Treatise on Electricity and Magnetism*; Oxford University Press: London, 1873; Vol. *1*.
(39) Wu, S. H. *Polymer* **1985**, *26* (12), 1855−1863.
(40) Rubinstein, M.; Colby, R. H. *Polymer Physics*; Oxford University Press: New York, 2003; p 440.
(41) Schneider, G. J.; Nusser, K.; Willner, L.; Falus, P.; Richter, D. *Macromolecules* **2011**, *44* (15), 5857−5860.
(42) Yamamoto, U.; Schweizer, K. S. *J. Chem. Phys.* **2011**, *135* (22), 224902.